Int. J. Electrochem. Sci., 14 **(2019)** 10213 – 10226, doi: 10.20964/2019.11.18

International Journal of
ELECTROCHEMICAL
SCIENCE
www.electrochemsci.org

Short Communication

Iron Corrosion in Occluded Water in Drinking Water Distribution Systems

Huiyan Tong[1,*], *Xingshuai Hu*[1], *Peng Zhao*[2,*], *Hongwei Zhang*[2], *Yimei Tian*[2]

[1] Dalian University of Technology, Panjin, China
[2] Department of Environmental Engineering, School of Environmental Science and Engineering, Tianjin University, Tianjin, China
[*]E-mail: tonghuiyan@dlut.edu.cn

Received: 5 July 2019 / *Accepted:* 14 August 2019 / *Published:* 7 October 2019

Corrosion in drinking water distribution systems is a serious problem and has attracted increasing attention. This work characterizes the iron corrosion in occluded water and provides a perspective of many pipeline leakage incidents, especially the hidden leakage in pipes. Corrosion products were analysed, and the corrosion rate and behaviour of cast iron were compared by potentiodynamic polarization and electrochemical impedance spectroscopy measurements in occluded water and flowing water separately. In addition, a conceptual model of iron corrosion demonstrated complex interactions. This work extends the knowledge of the corrosion mechanism for local corrosion and the propagation of water leakage.

Keywords: drinking water distribution systems; water leakage; iron corrosion; occluded water; electrochemistry

1. INTRODUCTION

Localized corrosion, or pitting corrosion, is a very damaging form of corrosion in drinking water distribution systems (DWDSs). Pitting corrosion can be concentrated on very small, fixed anode points. This attack remains unpredictable and eventually can penetrate the pipe wall.

Pitting corrosion is a cause of water leakage in DWDSs. Water leakage in DWDSs is a serious issue for many cities and increasingly attracts attention from governments, water industries, and research institutes [1, 2]. A substantial amount of water is lost in buried distribution networks due to water leakage. Specifically, more than 32 billion m^3 of potable water is lost from water distribution networks all over the world annually, which accounts for 35% of the total amount of water supplied [3]. In addition to the loss of treated water, water leakage causes energy waste and major socio-economic losses, degrades

water utilities' public reputation, and increases the risk of drinking water pollution (which represents a health threat to water consumers) [1, 3]. Furthermore, the development of small cracks in pipes, if not detected, may lead to pipe bursting and other severe consequences. Therefore, the control of water leakage is a major objective for water industries, and there is a vital need to understand the pitting corrosion in DWDSs.

The corrosion of cast iron is a very complex phenomenon that involves many factors within a given distribution system, including the materials, operating conditions, water chemistry, microbial activity, and other variables. Many researchers have studied the influence of water quality parameters (e.g., pH, oxygen, alkalinity, chloride, sulfate, temperature) [4-7], operating conditions (e.g., stagnation) [8, 9] and biofilms [10, 11] on corrosion and iron release into drinking water. Many studies have been performed to understand the mechanism of corrosion for iron and steel in various systems [12-15]. However, fully understanding the process is still a challenge to researchers, and the complexity of the phenomena does not allow a general mechanism to be established yet.

As pipes age and corrosion continues, the pipe failure frequency tends to increase. The pitting corrosion tends to grow under the cast iron surface, leaving a porous metallic cover layer [16]. The corrosion product internal calculated porosity is 40–54% [17]. The porous core consists of solid and fluid, and the fluid in the corrosion product is completely different from the flowing water. Baylis made this discovery in 1926 and noted that the water in the interior of the tubercle had much lower pH and a higher concentration of chloride and sulfate than that of the flowing water [18]. Tuovinen et al. [19] and Nawrocki et al. [20] confirmed these facts. According to Nawrocki et al. [20], the water surrounding the corrosion products in the pipe and in the interior of the corrosion products had reductive properties and relatively high concentrations of iron, manganese and chloride. In our previous study [21], occluded water – the water that remains in corrosion products' interiors – was acidic and had high concentrations of iron, chloride, and sulfate. Previous studies showed that once an iron pipe was installed in a DWDSs, corrosion would occur quickly during the first few years and then slow [17, 22]. After a typical product had formed, further corrosion of the corroded floor proceeded slowly [23]. However, corrosion develops on the inner surfaces of the pipes. The corrosion rate after activation is affected by the accessibility and quality of the water (e.g., pH, oxygen, alkalinity, chloride, sulfate, temperature) at the corroding metal [24]. The solution medium that the corroded floor contacts directly is occluded water, whose properties are quite different from those of flowing water. It is therefore unclear whether the corrosion rate of iron is accelerated or inhibited in the occluded water. In addition, numerous research papers have been dedicated to understanding the corrosion processes of corrosion in flowing water [25] and the pitting corrosion in simulated pore solutions [13]. However, the local corrosion in occluded water obtained from actual drinking water cast iron pipes has not been understood. Moreover, very few studies have focused on why and how natural ageing and corrosion of pipes cause water leakage. Hence, there is a vital need for research on iron corrosion in occluded water in DWDSs.

This paper analysed the morphology and composition of corrosion products in DWDSs and compared the corrosion rate and the corrosion behaviours of cast iron by potentiodynamic polarization and electrochemical impedance spectroscopy (EIS) measurements in two different media: occluded water and flowing water. Based on the results of the quality of occluded water and the corrosion behaviour of cast iron in occluded water, a conceptual model of iron corrosion in the occluded water was

proposed. This work extends the knowledge of the corrosion mechanism for local corrosion in DWDSs and makes an important contribution to a better understanding of the propagation of water leakage.

2. EXPERIMENTAL

2.1. SEM and XRD

The corrosion products were sampled from a corroded cast iron pipe that was used in a DWDSs for approximately 30 years. The finished water supplied by the corroded cast iron pipe has relatively high alkalinity and total hardness, and the pH of the finished water varies from 7.0 to 8.5. Some product samples were saved for scanning electron microscope (SEM) analysis, and some were pretreated for X-Ray diffraction (XRD). The samples were pulverized and then vacuum freeze-dried [26]. The morphology of the corrosion products was examined using SEM (PHILIPS XL-30 TMP, Netherlands), and XRD measurements (D/MAX-2500, Japan) were performed to identify the predominant mineralogical phases. The XRD operation parameters were as follows: Cu Kα radiation at 40 kV and 100 mA, 2θ ranging from 10° to 75° with a 0.02° step, and a 5 s count time at each step. The crystalline phase was identified using the Jade XRD software.

2.2. Electrochemical Measurements and Materials

The formation of occluded water is the result of localized corrosion, which is depicted by the occluded corrosion cavity (OCC) model [16, 27]. Thus, an OCC simulation cell was designed according to a previous study [28]. A schematic diagram of the designed OCC simulation cell is shown in Fig. 1a, and a diffusion channel is shown in Fig. 1b. The OCC cell was made from polytetrafluoroethylene and organic glass. The corrosion products filled in the diffusion channel were collected from a cast iron pipe used in a DWDSs with a considerable concentration of iron oxides and calcium carbonate. Electrochemical measurements were carried out in a conventional three-electrode electrochemical cell. The working electrodes were made of cast iron. Prior to each experiment, the surface of the working electrodes was polished with emery paper to 2000 grit and then cleaned with distilled water, degreased with ethanol, and finally dried. The working electrodes in occluded water and drinking water had exposed areas of 0.2 cm^2 and 1 cm^2, respectively.

The electrolyte in the OCC simulation cell was 1.2 mL of occluded water. The electrolyte in the bulk was flowing water. The occluded water was sampled from corrosion products' interiors of a cast iron pipe used in a DWDSs. The method of occluded water collection was the same as that of Huiyan et al. [21]. Flowing water was taken directly from the distribution system of the city of Tianjin. The occluded and drinking water samples were filtered with a 0.45 μm membrane and diluted to different concentrations for analysis of inorganic ions and metal ions. The inorganic anions (Cl^-, SO_4^{2-}, NO_3^-) were determined by ion chromatography on a DIONEX DX-600 system. The metal ions (Fe, Na, Mg, K, Ca, Mn, Zn, Sr) were determined by inductively coupled plasma mass spectrometry (ICP-MS). The main physicochemical parameters of the two kinds of water are listed in Table 1. The sampling process

may lead to an increase in dissolved oxygen, so the occluded water was deoxygenated by nitrogen before the experiment began. The cell was connected to a storage vessel (approximately 20 L) using a silicone flexible hose and a peristaltic pump. The flowing water was circulated continuously during the experiment at a flow velocity of 0.3 m/s. All experiments were performed at room temperature.

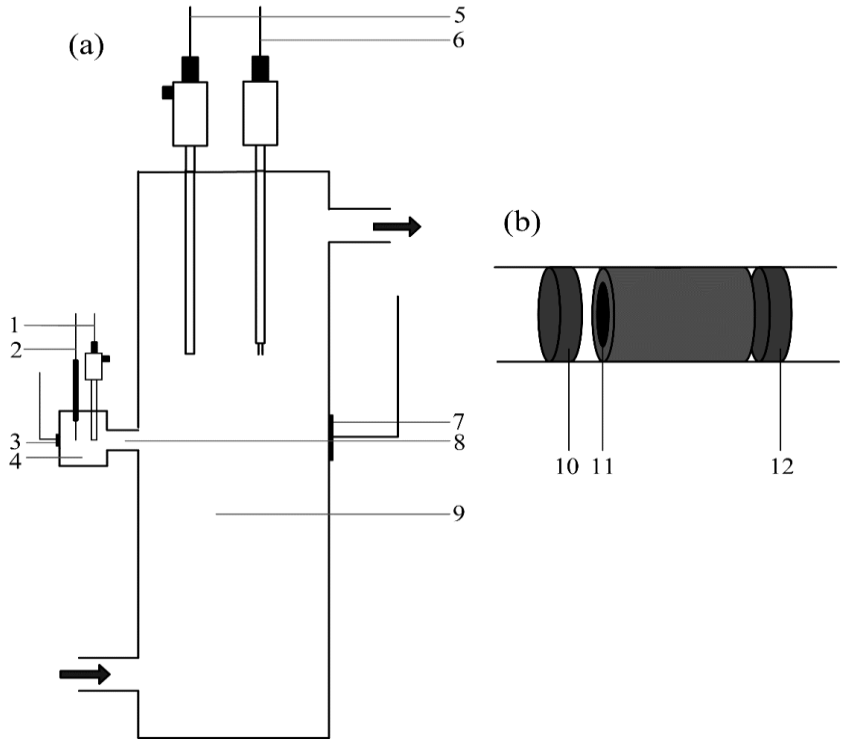

Figure 1. A schematic diagram of the OCC simulated cell (a) and diffusion channel in the OCC (b). 1, 5-saturated calomel electrodes (SCEs), 2-platinum wire electrode, 3, 7-working electrodes, 4-occluded water, 6-platinum foil electrode, 8-diffusion channel, 9-drinking water, 10, 12-filter papers, and 11-corrosion products.

Table 1. Properties of flowing water and occluded water

Properties	Flowing water	Occluded water
pH	7.42	5.01
Dissolved iron [a]	0.05274	823.2
Na [a]	22.41	19.27
Mg [a]	20.95	18.78
Ca [a]	3.541	3.233
K [a]	5.440	4.464
Zn [a]	0.02803	0.2173
Mn [a]	0.05103	2.563
Sr [a]	0.3032	0.2138
Cl^- [a]	53.11	645.6
SO_4^{2-} [a]	113.3	1173
NO_3^- [a]	4.615	5.608
Dissolved oxygen [a]	6.53	1.63
a Concentration unit: mg/L.		

2.3. Electrochemical techniques

The potentiodynamic polarization and EIS measurements were carried out in the OCC cell using a CS354 electrochemical workstation. All the potentials in this work are referenced to an SCE. The counter electrodes are a platinum wire and a platinum foil in occluded water and flowing water, respectively. For potentiodynamic polarization experiments, the potential was scanned from -0.01 to 1 V at a scan rate of 0.1667 mV/s, and the experiment was ceased when the anode current was greater than 1 mA. EIS measurements were performed at the open-circuit potential with a 5 mV amplitude signal, and data were collected in a frequency range of 100 kHz to 0.01 Hz using 8 points per decade. The impedance curves were fitted to equivalent electric circuit models, and the characteristic parameters were determined using the ZSimpWin software.

3. RESULTS AND DISCUSSION

3.1. SEM and XRD analysis of corrosion products

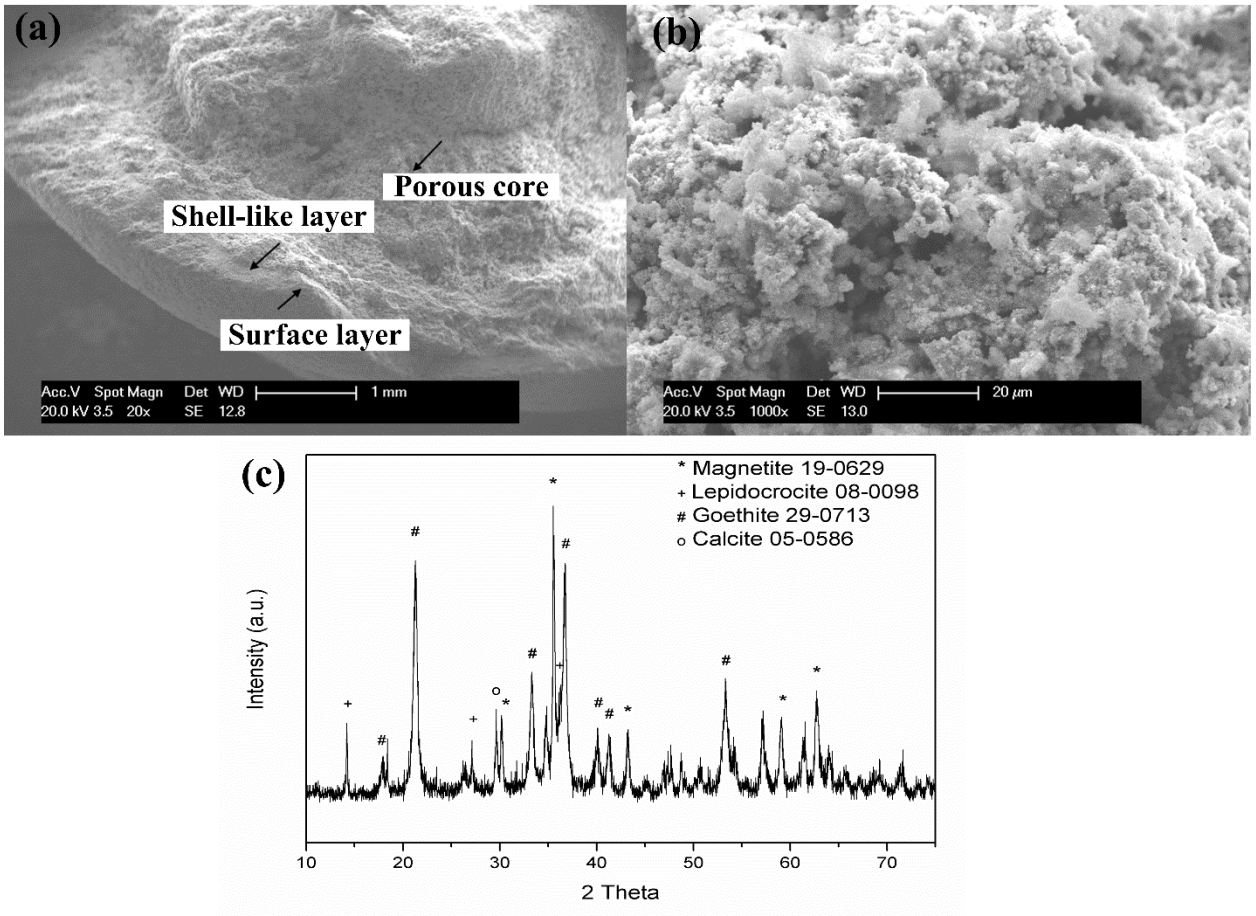

Figure 2. SEM images of the iron pipe corrosion product: corrosion product cross section (×20) (a) and porous core section (×1000) (b), and XRD pattern of the iron pipe corrosion product (c).

The SEM images of the corrosion products from the cast iron pipe used in a DWDSs for approximately 30 years are shown in Fig. 2a, b. The morphology of the corrosion products was consistent with earlier reports [29]. The corrosion products had characteristic features that include the following: (1) a surface layer, (2) a relatively dense shell-like layer, and (3) a porous core that contains occluded water. The composition of the corrosion products was analysed by XRD (Fig. 2c). XRD analysis showed a complex mixture: goethite (α-FeOOH), lepidocrocite (γ-FeOOH), magnetite (Fe_3O_4) and calcite ($CaCO_3$). The observed iron (hydr)oxide minerals were in good agreement with results obtained previously [23, 26, 30].

3.2. Potentiodynamic polarization curves

The porosity of the corrosion products leads to the formation of an occluded environment under the scales that contains occluded water. Previous studies showed that the corrosion rates of metals were initially high and decreased rapidly as the scale layer grew [17, 22]. After a typical scale had formed, further corrosion of the corroded floor proceeded at a slow rate [23]. However, corrosion develops on the inner surfaces of the pipes, and when the corrosion products grow, occluded water develops. The solution medium that the corroded floor contacts directly is occluded water, whose properties are quite different from those of flowing water. The chemistry of the solution inside the corrosion products should play a significant role (at least on a local scale) [31]. Occluded water is an acidic environment, with high concentrations of iron, chloride, sulfate, nitrate and manganese (Table 1). It is therefore convoluted and quantitatively unclear whether the anodic dissolution of Fe is accelerated or inhibited in the occluded water at local anode sites. Therefore, in this study, the corrosion rate of cast iron in occluded water was measured and compared with that in flowing water.

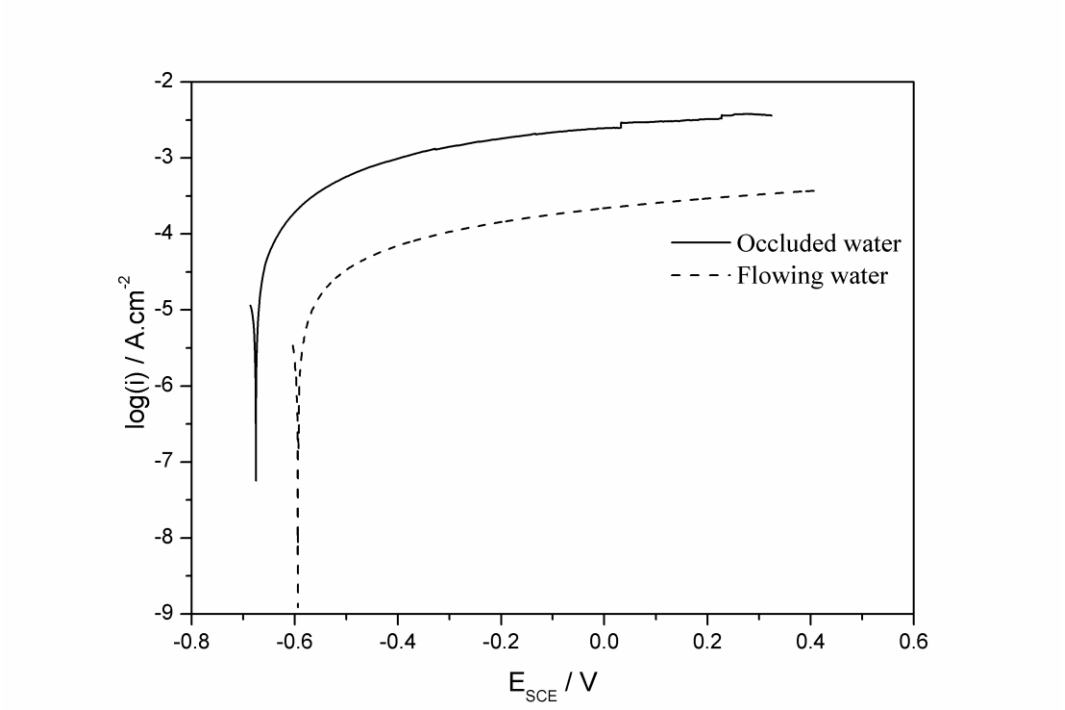

Figure 3. Potentiodynamic polarization curves of cast iron in occluded water and flowing water.

Potentiodynamic polarization curves of cast iron in flowing water and occluded water are shown in Fig. 3. No obvious active-passive transition potential peaks were observed in flowing water or occluded water, indicating aggressive behaviour in these two solutions. The anodic current densities increase rapidly with increasing corrosion potential (E_{corr}) values and then increase slowly. This behaviour is attributed to the ions attacking the surface, leading to anodic dissolution of the material and continuation of the corrosion process, maintaining the surface active state.

The E_{corr} values considered in the work were derived from these curves. To calculate the corrosion current density, the Tafel procedure was used. Finally, the corrosion rate values were calculated based on Faraday's law using Eq. 1 [9]:

$$v = \frac{3.27 i_{corr} M}{n\rho} \quad \text{(Eq. 1)}$$

where the corrosion rate is represented by v (μm/y), the corrosion currents are represented by i_{corr} (μA/cm^2), the atomic mass of metal (g) is represented by M, the density of the metal is represented by ρ (g/cm^3), and the number of electrons lost per atom oxidized is represented by n. The electron number was 2 for cast iron to determine the corrosion rate.

The E_{corr} and i_{corr} values were determined by extrapolating the anodic Tafel region [32]. The occluded water is stagnant compared to flowing water, and studies have shown that E_{corr} decreases significantly and consistently during stagnation episodes [33]. From our results, we can see that the E_{corr} value in the occluded water shifted in the negative direction compared with that in the flowing water. This result may be related to a greater activity of the iron. The concentrated chloride and sulfate ions in the occluded water reached the metal/film interface and formed adsorbed intermediates, increasing the activity of the cast iron. In addition, the flow state affected the mass transfer. The different flow state between occluded water and flowing water also affected the potential of the cast iron. The results showed that the corrosion rate of cast iron in occluded water was approximately 5500 μm/y and approximately 600 μm/y in flowing water. This finding clearly indicates that the occluded water, with low pH and high concentrations of iron, chloride, and sulfate, is more aggressive than flowing water in terms of electrochemical corrosion, and the corrosion rate is increased in occluded water. This phenomenon may greatly reduce the service life of pipelines. For the majority of large and medium-sized cities in China, the average leakage ratio was relatively high [1]. Therefore, many pipeline leakage accidents must be highly related to the high corrosion rate of cast iron in occluded water.

3.3. Electrochemical impedance analysis of the behaviour of cast iron in occluded water and in flowing water

The corrosion behaviour of cast iron in occluded water was analysed and compared with that in flowing water. The Nyquist plots and Bode plots of cast iron in flowing water are shown in Fig. 4a, c. The impedance diagram can be described by two loops, one high-frequency capacitive loop and one low-frequency capacitive loop. The high-frequency loop was attributed to a film capacitance [34] with a very small value (1.2×10^{-9} F/cm^2). The low-frequency capacitive loop was associated with diffusion impedance [34].

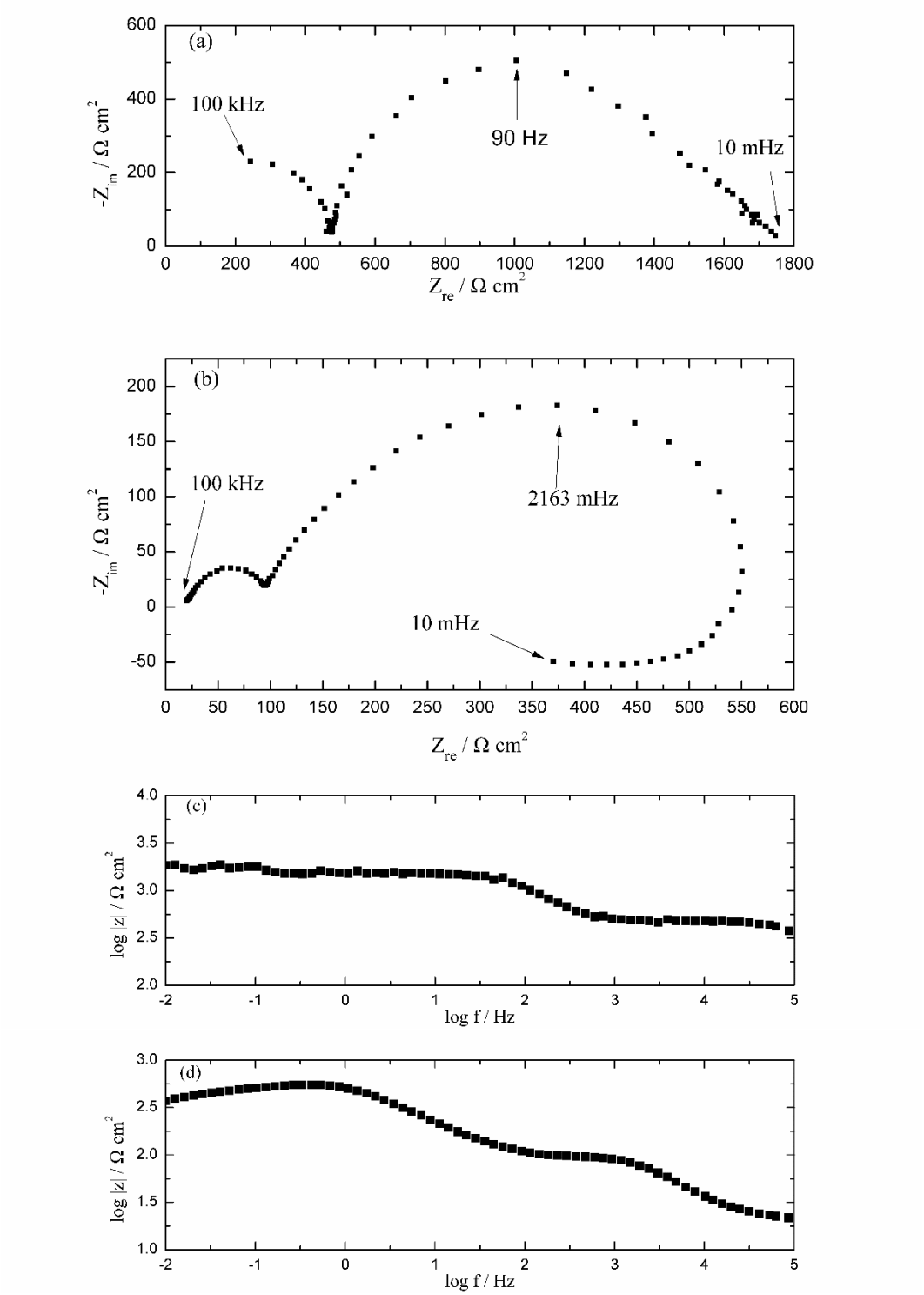

Figure 4. Nyquist plots of cast iron in flowing water (a) and occluded water (b), and Bode plots of cast iron in flowing water (c) and occluded water (d).

The equivalent electric circuit of cast iron immersed in flowing water is shown in Fig. 5a. Because electrochemical systems present different types of inhomogeneities, constant phase elements (*CPE*s) describe capacitive behaviour better than capacitors in the equivalent circuit [9, 35, 36]. The pseudocapacitance (*C*) associated with the *CPE* can be calculated using Eq. 2.

$$C = \frac{(Y_0 R)^{1/n}}{R} \quad \text{(Eq. 2)}$$

where the pseudocapacitance associated with the *CPE* is represented by *C*, the constant with dimensions of S.sn/cm^2 is represented by Y_0, and the electrical resistance in parallel with the *CPE* is represented by *R* [9].

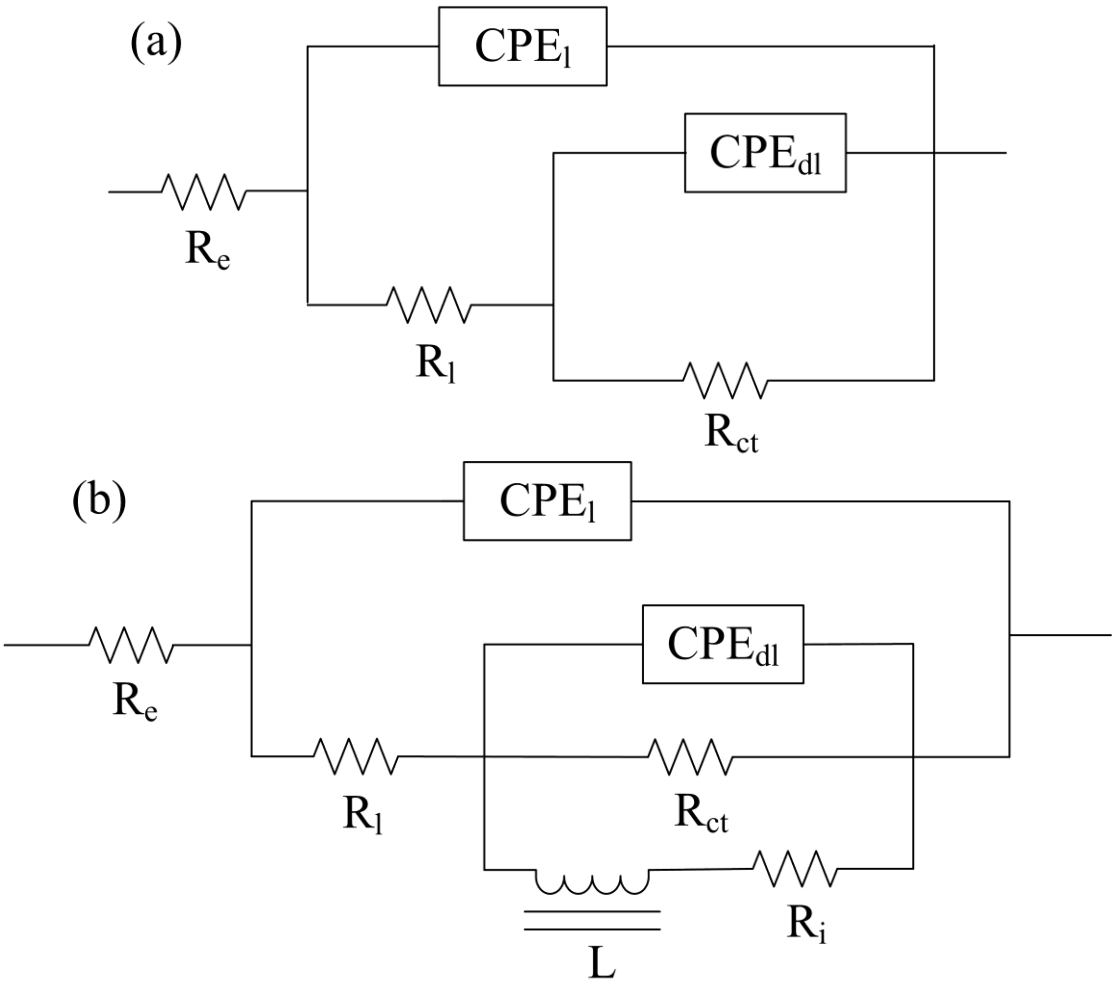

Figure 5. Physical model and equivalent circuits used to fit the impedance spectra of cast iron in flowing water (a) and occluded water (b).

In the circuit of Fig. 5a, R_e represents the electrolyte resistance, CPE_l is the constant phase element related to the film, R_l is the resistance of the film, CPE_{dl} is the constant phase element related to the double-layer capacitance, and R_{ct} is the charge-transfer resistance. The value of R_{ct} (approximately 2700 Ω cm^2) is in good agreement with the result of R_p (approximately 2500 Ω cm^2) obtained by the potentiodynamic polarization curves.

The Nyquist plots and Bode plots of cast iron in occluded water are shown in Fig. 4b, d. The impedance diagram is different from that of the flowing water. The diagram can be described by three loops, namely, one high-frequency capacitive loop, one medium-frequency capacitive loop and one short low-frequency inductive loop. The high-frequency loop characterized by a very small capacitance was

attributed to film capacitance. This capacitance may correspond to a surface film of insoluble corrosion products acting as a discontinuous dielectric layer [9]. In fact, the capacity (5.5×10^{-7} μF/cm^2) associated with this loop was much lower than the normal double-layer capacitance value (between 10 μF/cm^2 and 40 μF/cm^2) [9]. The medium-frequency capacitive loop resulted from diffusion through the porous surface film [36]. The inductive loop may be related to the adsorption of an intermediate product $FeOH_{ads}$ on the metal surface [37-39].

In addition, regarding the influence of chloride ions on the impedance responses of iron electrodes in acidic solution, Barcia and Mattos [40] and Itagaki et al. [41] reported that the inductive behaviour in the Nyquist plot was influenced by the presence of chloride ions. Chloride ions reached the metal/film interface and formed an adsorbed intermediate with iron ions $FeCl_{ads}$. These processes all represented the active dissolution of the metal surface.

To estimate the physical parameters of the impedance of cast iron immersed in occluded water, the equivalent electric circuit (Fig. 5b) was used. The use of this equivalent circuit, in which a diffusion branch appeared, conveyed the idea that the iron oxide layer allowed the diffusion of species through it [9]. In the circuit of Fig. 5b, R_e represents the electrolyte resistance, CPE_l is the constant phase element related to the film, R_l is the resistance of the film, CPE_{dl} is the constant phase element related to the double-layer capacitance, R_{ct} is the charge-transfer resistance, L is the inductance, and R_i is the resistance of the inductance. It is considered that the anodic branch of the impedance corresponds to a charge-transfer resistance R_{ct} (approximately 340 Ω cm^2). This value is also in good agreement with the result of R_p (approximately 370 Ω cm^2) obtained by the potentiodynamic polarization curves. The value of R_{ct} in occluded water is much lower than that in flowing water, which indicates that corrosion may become easier in occluded water.

3.4. Iron corrosion in the occluded water

The positive results of the polarization studies and EIS studies in the occluded water confirmed the high dissolution rate of Fe in the occluded water. In addition, the corrosion behaviour of cast iron in occluded water was different from that in flowing water. To explain these results, a schematic representation of different corrosion reactions in the occluded water is proposed, as presented in Fig. 6. The tuberculation corrosion proceeds with the formation of corrosion cells, the anode site under the corrosion products and the relatively large cathode site around the corrosion products, owing to the difference in the oxygen supply. The properties of the corrosion products play an important role in the corrosion processes. Previous studies have shown that corrosion products exhibit electrical conductivity, porosity, ion selectivity, and oxidation and deoxidization capability [42-45]. Because the corrosion products possess electrical conductivity, the anodic reaction inside the corrosion products and the oxygen reduction reaction outside of the corrosion products can form a corrosion cell. The porosity of the corrosion products leads to the existence of occluded water and affects the migration of dissolved oxygen and ions. The role of selective ion transport through the corrosion products also affects the migration of ions between occluded water and flowing water. As shown in Fig. 6, the main anodic reaction is the oxidation of iron in occluded water, and the main cathodic reaction is oxygen reduction on the outside

of the corrosion products. Fe^{2+} is generated by the anodic reaction ($Fe \rightarrow Fe^{2+} + e$) at the local anode site. The migration of Fe^{2+} to the flowing water is restricted due to the corrosion products [46], and Fe^{2+} is enriched in the occluded water. Then, Fe^{2+} is hydrolysed, and as a result, the pH at the local anode site decreases. Although the diffusion of dissolved oxygen from the flowing water towards the occluded water is disturbed by the corrosion products, low concentrations of dissolved oxygen may be present in the occluded water [17], and oxygen is readily consumed to oxidize Fe(II) to Fe(III) in the occluded water. The Fe(II) complexes may be present in solution or adsorbed on solid phases. The oxidation and hydrolysis of Fe(II) can form Fe(III) oxides. The Cl^- and SO_4^{2-} are transported to the local anodic site by electrophoresis through corrosion products via anion-selective transport and accumulate in the occluded water. Generally, anions such as Cl^- and SO_4^{2-} can accelerate corrosion by promoting anodic dissolution, probably in a manner similar to some kind of catalysis [47]. Additionally, the concentrated Cl^- ions can form an adsorbed intermediate, which causes the inductive loop in the impedance diagrams. The concentrated Cl^- ions not only can accelerate the dissolution of iron as mentioned above but also may contribute to the increased activity coefficient of H^+ and accelerated hydrolysis of Fe^{2+}, as shown in the following reactions [48].

$$Fe^{2+} + 2Cl^- + 4H_2O \rightarrow FeCl_2 \cdot 4H_2O \quad \text{(Eq. 3)}$$

$$FeCl_2 \cdot 4H_2O \rightarrow Fe(OH)_2 + 2Cl^- + 2H^+ + 2H_2O \quad \text{(Eq. 4)}$$

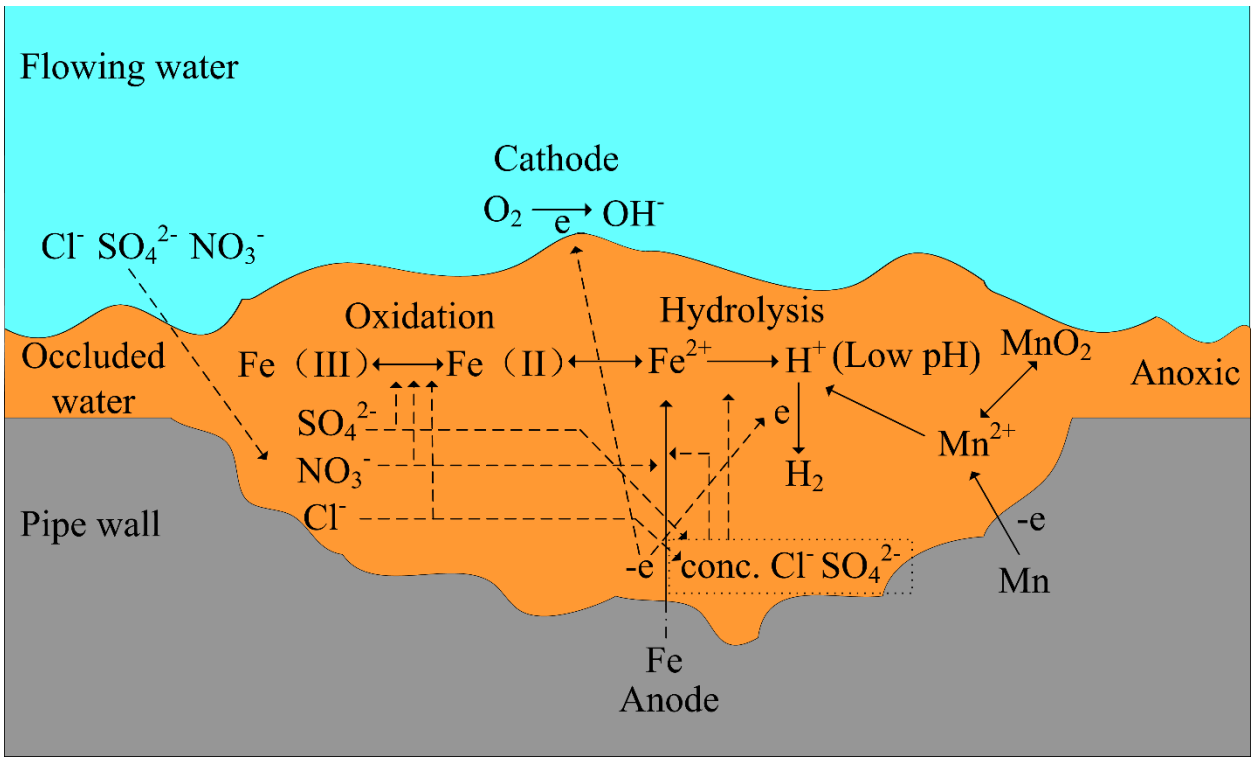

Figure 6. Schematic representation of different corrosion reactions in the occluded water.

In addition, NO_3^- can oxidize Fe^0 in occluded water with a low pH [49]. The migration of H^+ to the flowing water is also restricted due to the corrosion products, and H^+ is enriched in the occluded

water, leading to a decreased pH. In addition, H_2 may be generated in occluded water, and this process contributes in part to the entire anodic reaction.

The high concentration of Mn may also cause this metal to be incorporated into the corrosion process. Mn may be released from the cast iron pipe, and this process may also contribute to the entire anodic reaction. It is well known that the oxidation of Mn^{2+} in acidic media can follow these elementary steps [50, 51]:

$$Mn^{2+} \rightarrow Mn^{3+} + e^- \quad \text{(Eq. 5)}$$

$$Mn^{3+} + H_2O \rightarrow MnOOH + 3H^+ \quad \text{(Eq. 6)}$$

$$MnOOH \rightarrow MnO_2 + e^- + H^+ \quad \text{(Eq. 7)}$$

Mn^{3+} may either disproportionate to Mn^{2+} and Mn^{4+} at low acid concentrations, as given by the following reaction [52]:

$$2Mn^{3+} \rightarrow Mn^{2+} + Mn^{4+} \quad \text{(Eq. 8)}$$

$$Mn^{4+} + 2H_2O \rightarrow MnO_2 + 4H^+ \quad \text{(Eq. 9)}$$

Therefore, the pH in the occluded water may also be affected by the hydrolysis of Mn^{3+} or Mn^{4+}. MnO_2 can oxidize Fe^{2+} [53].

4. CONCLUSIONS

The corrosion behaviour of iron was determined by potentiodynamic polarization and EIS measurements in occluded water and flowing water. The results demonstrate that the occluded water is more corrosive than the flowing water with respect to electrochemistry. The occluded water, with low pH and high concentrations of Cl^- and SO_4^{2-}, risks penetrating the pipe wall and causing pipe network leakage, especially hidden leakage. The EIS results show that the corrosion behaviour of cast iron in occluded water is different from that in flowing water. In both occluded water and drinking water, the diffusion impedance is associated with the inner oxide film. However, in occluded water, an inductive loop appeared in the impedance diagrams, indicating that intermediate products are generated and adsorbed on the iron surface during the corrosion process. The formation of these intermediate products makes the iron oxidation reaction easier. However, in this paper, only the electrochemical properties of the occluded water are considered, and microbial corrosion should be studied in the future to better understand the corrosion in the occluded water. Overall, the results of this work extend the knowledge of the local corrosion mechanism in DWDSs and make an important contribution to a better understanding of the propagation of water leakage.

ACKNOWLEDGMENTS

This work was supported by the National Natural Science Foundation of China [grant numbers 51608093, 51208353] and “the Fundamental Research Funds for the Central Universities” [grant numbers DUT15RC(3)102, DUT18RC(4)062]. We also thank Ke Wang and Xuehui Wang for their help.

References

1. W. Li, W. Ling and S. Liu, *J. Environ. Sci*., 23 (2011) 1816.
2. S. D. Miranda, L. Molari and G. Scalet, *Eng. Struct.*, 79 (2014) 142.
3. Q. Xu, R. Liu and Q. Chen, *J. Environ. Sci.*, 26 (2014) 955.
4. H.Y. Ma, C.Y. Yang and G.Y. Li, *Corrosion*, 59 (2003) 1112.
5. A. Sander, B. Berghult and E. Ahlberg, *Corros. Sci.*, 39 (1997) 77.
6. P. Sarin, V.L. Snoeyink and J. Bebee, *Water Res*., 38 (2004) 1259.
7. C. Volk, E. Dundore and J. Schiermann, *Water Res.*, 34 (2000) 1967.
8. P.S. Husband and J.B. Boxall, *Water Res*., 45 (2011) 113.
9. J.F. Rios, J.A. Calderón and R.P. Nogueira, *Corrosion*, 69 (2013) 875.
10. F. Li, M. An and G. Liu, *Mater. Chem. Phys*., 113 (2009) 971.
11. B. Qi, B. Wang and W. Chenguan, *Int. J. Electrochem. Sci.*, 8 (2013) 1813.
12. M.I. Abdulsalam, *Corros. Sci.*, 47 (2005) 1336.
13. E.C. Paredes, A. Bautista, S.M. Alvarez and F. Velasco, *Corros. Sci.*, 58 (2012) 52.
14. S.G. Wang, M. Sun and P.C. Cheng, *Mater. Chem. Phys*., 127 (2011) 459.
15. A. Wiengmoon, J.T.H. Pearce and T. Chairuangsri, *Mater. Chem. Phys.*, 125 (2011) 739.
16. D. Sun, Y. Jiang and Y. Tang, *Electrochim. Acta*, 54 (2009) 1558.
17. P. Sarin, V.L. Snoeyink, D.A. Lytle and W.M. Kriven, *J. Environ. Eng.*, 76 (2004) 364.
18. J.R. Baylis, *J. - Am. Water Works Assoc.,* 15 (1926) 598.
19. O.H. Tuovinen, K.S. Button and A. Vuorinen, *J. - Am. Water Works Assoc.*, 72 (1980) 626.
20. J. Nawrocki, U. Raczykstanisławiak and J. Świetlik, *Water Res.*, 44 (2010) 1863.
21. H.Y. Tong, P. Zhao, H.W. Zhang, Y.M. Tian, X. Chen, W.G. Zhao and M. Li, *Chemosphere*, 119 (2015) 1141.
22. H. Sontheimer, W. Kölle and V.L. Snoeyink, *J. - Am. Water Works Assoc.*, 73 (1981) 572.
23. T. Borch, A.K. Camper and J.A. Biederman, *J. Environ. Eng.*, 134 (2008) 835.
24. M. Kouřil, P. Novák and M. Bojko, *Cem. Concr. Res.*, 40 (2010) 431.
25. M.R. Lasheen, C.M. Sharaby and N.G. El-Kholy, *J. Hazard. Mater.*, 160 (2008) 675.
26. F. Yang, B. Shi, J. Gu and D. Wang, *Water Res.*, 46 (2012) 5423.
27. G. Yang, L. Ying and H. Lin, *Corros. Sci*., 43 (2001) 397.
28. Y. Zhu, Y. Qiu and X. Guo, *J. Appl. Electrochem.*, 39 (2009) 1017.
29. T.L. Gerke, J.B. Maynard and M.R. Schock, *Corros. Sci*., 50 (2008) 2030.
30. M. Li, Z. Liu and Y. Chen, *Water Res.*, 106 (2016) 593.
31. C. Blanc, N. Pébère and B. Tribollet, *Corros. Sci.*, 52 (2010) 991.
32. H. Xu and A. Neville, *Wear,* 233 (1999) 523.
33. M. Fabbricino and G.V. Korshin, *Water Res.*, 62 (2014) 136.
34. M. Sancy, Y. Gourbeyre and E.M.M. Sutter, *Corros. Sci*., 52 (2010) 1222.
35. Y.S. Huang, X.T. Zeng and X.F. Hu, *Electrochim. Acta*, 49 (2004) 4313.
36. Y. Song, D. Shan and R. Chen, *Corros. Sci.*, 51 (2009) 1087.
37. F. Farelas, M. Galicia and B. Brown, *Corros. Sci*., 52 (2010) 509.
38. G.A. Zhang and Y.F. Cheng, *Corros. Sci.*, 51 (2009) 87.
39. G.A. Zhang and Y.F. Cheng, *Corros. Sci.*, 52 (2010) 2716.
40. O.E. Barcia and O.R. Mattos, *Electrochim. Acta*, 35 (1990) 1601.
41. M. Itagaki, M. Tagaki and K. Watanabe, *Electrochim. Acta*, 41 (1996) 1201.
42. S. Hœrlé, F. Mazaudier and P. Dillmann, *Corros. Sci.*, 46 (2004) 1431.
43. V. Lair, H. Antony and L. Legrand, *Corros. Sci.*, 48 (2006) 2050.
44. J. B. Memet, P. Girault and R. Sabot, *Electrochim. Acta*, 47 (2003) 1043.
45. J. Wielant, V. Goossens and R. Hausbrand, *Electrochim. Acta*, 52 (2007) 7617.
46. Y. Zhu and X. Guo, *J. Chin. Soc. Corros. Prot*., 5 (2008) 271.
47. X. Zhang, K. Xiao and C. Dong, *Eng. Failure Anal.*, 18 (2011) 1981.

48. M. Sun, K. Xiao and C. Dong, *J. Mater. Eng. Perform*., 22 (2013) 815.
49. J.M. Rodríguezmaroto, F. Garcíaherruzo and A. Garcíarubio, *Chemosphere,* 74 (2009) 804.
50. M. Chotkowski, Z. Rogulski and A. Czerwiński, *J. Electroanal. Chem*., 651 (2011), 237.
51. Z. Rogulski, M. Chotkowski and A. Czerwiski, *J. New Mater. Electrochem. Syst.*, 9 (2006) 333.
52. S. Nijjer, J. Thonstad and G.M. Haarberg, *Electrochim. Acta*, 46 (2000) 395.
53. D. Postma and C.A.J. Appelo, *Geochim. Cosmochim. Acta*, 64 (2000) 1237.